Letter | Editors' Suggestion

# Quantized interband topological index in two-dimensional systems

Tharindu Fernando [1,*] and Ting Cao [2]

[1]*Department of Physics, University of Washington, Seattle, Washington 98195, USA*

[2]*Department of Materials Science and Engineering, University of Washington, Seattle, Washington 98195, USA*

(Received 18 May 2023; revised 28 July 2023; accepted 1 August 2023; published 15 August 2023)

We introduce a novel gauge-invariant, quantized interband index in two-dimensional (2D) multiband systems. It provides a bulk topological classification of a submanifold of parameter space (e.g., an electron valley in a Brillouin zone), and therefore overcomes difficulties in characterizing topology of submanifolds. We confirm its topological nature by numerically demonstrating a one-to-one correspondence to the valley Chern number in $k \cdot p$ models (e.g., gapped Dirac fermion model) and the first Chern number in lattice models (e.g., Haldane model). Furthermore, we derive a band-resolved topological charge and demonstrate that it can be used to investigate the nature of edge states due to band inversion in valley systems like multilayer graphene.

DOI: 10.1103/PhysRevB.108.L081111

*Introduction.* Topological and geometric effects are being heavily investigated in contemporary condensed matter physics. For an adiabatic evolution along a closed loop in a 2D parameter space, the geometric part of the final electronic eigenstate's phase is U(1) gauge-invariant (modulo $2\pi$). This Berry phase contribution depends solely on the geometry of the parameter space [1]. The corresponding Berry curvature is a geometrically local quantity, which when summed over the entire 2D-space manifold, may yield topological quantities such as the first Chern number [2–4]. In solid state physics, the Berry phase also plays vital roles in topology-related phenomena, and applications including electric polarization, orbital magnetism, adiabatic charge pumping, various types of Hall effects, and edge state engineering [5,6].

Despite these advancements, the understanding of the multilevel topology of parameter-space submanifolds is arguably still under development. This Letter will focus on $k$-space submanifolds in the vicinity of band edges at high-symmetry points (or so-called *valleys*) [7]. These valley degrees of freedom play key roles in future electronics and quantum information science, as quasiparticles residing in the valleys may carry information much like charge and spin [7–27]. The associated topology is currently studied using the *valley Chern number*. This is usually calculated using a loop integral of the Berry connection (a method that is arguably restrictive due to requiring a nonsingular gauge) or by integrating Berry curvature, in the vicinity of a valley [5]. Generally, both $k \cdot p$ and lattice models have proven useful in the study of topological phenomena of valleys. However, in $k \cdot p$ models, the area of Berry curvature integration required to obtain quantized valley Chern number is infinite (or equivalently, requires an infinitesimally small band gap [5,7,22]). On the other hand, in lattice models, there is no general quantized character to describe valley topology when the Berry curvature is not peaked at the valley; at least not without low-energy expansions or additional synthetic dimensions [6,28]. In addition, relating existing bulk indices to edge modes by the bulk-edge correspondence often requires summing the valley Chern number over all filled bands [5], and/or downfolding multiband Hamiltonians into simpler models [29–31]. This may cause a loss of information on the topological origin of edge states. For example, if the edge state arises from inverting a pair of bands among many bands, such band-resolved information would be missing in the valley Chern number description.

In this Letter, we introduce a new topological index $\Theta$, and the *interband frequency*; a correction term that keeps $\Theta$ quantized. Our approach gives us a *meaningful* topological valley index using a *finite* $k$-space integration, in *both* $k \cdot p$ and lattice models. We also present a band-resolved topological charge $\Xi$, that identifies orbitals associated with band inversions *without* downfolding multiband Hamiltonians.

*Interband index in 2D.* Consider the time-independent Schrödinger equation for an $N$-level nondegenerate Hamiltonian $H(\boldsymbol{k})$ over 2D parameter space $k$: $H(\boldsymbol{k})\,|m(\boldsymbol{k})\rangle = E_m(\boldsymbol{k})\,|m(\boldsymbol{k})\rangle$ $(m = 1, 2, \ldots, N)$, where $|m\rangle$ are orthonormal instantaneous eigenstates with eigenvalues $E_m(\boldsymbol{k})$. For an adiabatic evolution along a closed $k$-space loop $\partial\mathcal{M}$, we define the interband index $\Theta_{\boldsymbol{k}}$, following the definition of the *interlevel character* in Ref. [32]:

$$2\pi\,\Theta_{mn} = \Delta\Phi_{mn} - \oint_{\partial\mathcal{M}} d\arg\langle m \,|\, \nabla_{\boldsymbol{k}} n\rangle \cdot \hat{e}_\tau, \qquad (1)$$

Above, we used the definitions: $\boldsymbol{k} = (k_x, k_y)$; $d$ is the total derivative with respect to $k_x$ and $k_y$; $\nabla_{\boldsymbol{k}} = (\partial_{k_x}, \partial_{k_y})$; $\hat{e}_\tau = \dot{\boldsymbol{k}}/|\dot{\boldsymbol{k}}|$ is the unit tangential operator at a point on the loop $\partial\mathcal{M}$ [see Fig. 1(b)]; $\dot{\boldsymbol{k}} = d\boldsymbol{k}(\lambda)/\,d\lambda$ for some $\lambda$ that parameterizes the loop $\boldsymbol{k} = (k_x(\lambda), k_y(\lambda))$; and $\Delta\Phi_{mn} = \Phi_m - \Phi_n$, where $\Phi_m = \int_{\partial\mathcal{M}} \mathcal{A}_m^\mu\, d\lambda_\mu - \iint_{\mathcal{M}} F_m\, d\lambda_\mu\, d\lambda_\nu$. For brevity, we henceforth drop the differential elements $d\lambda_\mu$. $\Phi_m$ is the number of *Berry singularities* in level $|m\rangle$: It is the difference between the the line integral of the standard Berry connection $\mathcal{A}_m^\mu = i\,\langle m|\frac{\partial}{\partial\lambda_\mu} m\rangle$ along $\partial\mathcal{M}$, and the area integral of the

*tharindu@uw.edu

 

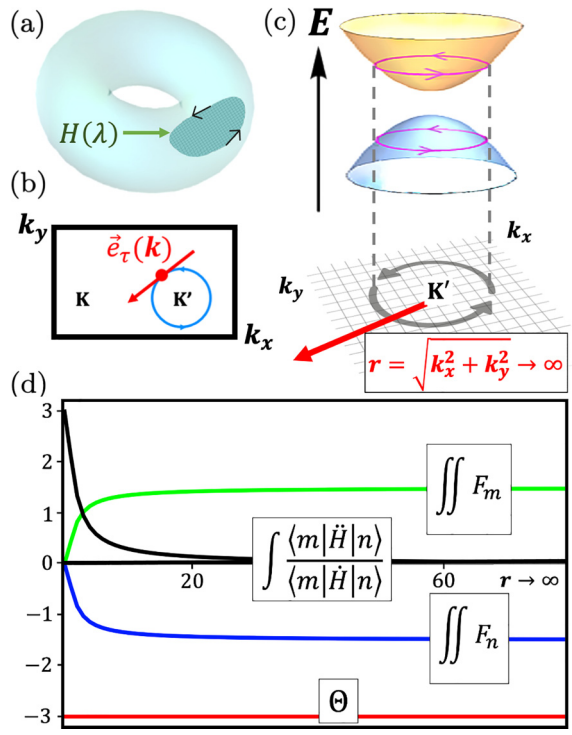


FIG. 1. (a) 2D $k$-space Brillouin torus for a two-level system. The counterclockwise closed loop is $\partial\mathcal{M}$, and defines the shaded region of the torus as $\mathcal{M}$, by convention. For a $k$-space loop parameterized by $\lambda$, the adiabatic evolution is given by $H(\lambda) \equiv H(\boldsymbol{k})$. (b) For $k$ constrained to $\partial\mathcal{M}$, the tangential vector $\vec{e}_\tau(k)$ at a point is denoted in red. $K$ and $K'$ are high-symmetry points. (c) Two energy levels of the dispersion $\boldsymbol{E}$ in the vicinity of the $K'$ valley. The red arrow schematically illustrates how the gray $k$-space loop's radius $r$ is increased in (d). (d) Berry curvature area integrals of upper and lower bands, integral of interband frequency, and the interband index in Eq. (2) as we vary the size of $k$ loops using $r$.

Berry curvature $F_m = \frac{\partial}{\partial\lambda_\mu}\mathcal{A}_m^\nu - \frac{\partial}{\partial\lambda_\nu}\mathcal{A}_m^\mu$ over the region $\mathcal{M}$ specified by the loop. So, $\Phi_m$ could be interpreted as the quantized "amount" by which Stokes' theorem fails. Then, $\Delta\Phi$ is the net number of Berry singularities between the levels considered. Notice that in the case without gauge singularities, $\Phi_m$ reduces to 0 as $\int_{\partial\mathcal{M}} \mathcal{A}_m^\mu = \iint_{\mathcal{M}} F_m$.

Following the derivation in Sec. A of Ref. [33], $\Theta_{mn}$ may be written as

$$2\pi\,\Theta_{mn} = \iint_{\mathcal{M}} F_n - \iint_{\mathcal{M}} F_m - \oint_{\partial\mathcal{M}} \mathrm{Im}\frac{\langle m|\ddot{H}|n\rangle}{\langle m|\dot{H}|n\rangle} - \oint_{\partial\mathcal{M}} \sum_{q\neq m,n} \frac{1}{E_{nq}}\left(2 - \frac{E_{nm}}{E_{qm}}\right)\mathrm{Im}\frac{\langle m|\dot{H}|q\rangle\langle q|\dot{H}|n\rangle}{\langle m|\dot{H}|n\rangle}. \tag{2}$$

The overhead dots represent derivation with respect to parameter $\lambda$. All terms in Eq. (2) are gauge-independent, and so, potentially observable. The first two terms in the right-hand side of Eq. (2) make the difference between the Berry curvature integrals. The third boundary term includes $\langle m|\ddot{H}|n\rangle/\langle m|\dot{H}|n\rangle$, which we call the *interband frequency*, since it resembles the ratio of an accelerationlike quantity to a velocitylike quantity. Since $k \to \infty$ implies the loop parameter (e.g., time) $\lambda \to \infty$, we intuit that the frequency ($\propto 1/\lambda$) $\to 0$. We show later in Fig. 1(d) that as $k \to \infty$, this correction term also tends to 0 in our numerical calculations on two-band models. To our knowledge, the interband frequency is new to the literature. Due to its dependence on the tangential vector $\hat{e}_\tau$, a unique vector field may be defined only *after* a loop is chosen. This makes the individual terms in the interband frequency ratio differ from existing quantities in the literature (such as the interband acceleration in second order nonlinear responses [34,35]).

The physical significance of the interband index thus becomes clear: it is a quantized topological character for a submanifold of 2D parameter space that depicts the difference between the Berry phases of a pair of bands, corrected by the interband frequency and other terms. Next, we demonstrate the physical meaning and applications of the interband index in $k \cdot p$ and lattice models.

*Application to the gapped Dirac fermion model and Haldane model.* We first calculate $\Theta$ and compare it with existing topological characterizations of $k \cdot p$ models. While we use the gapped Dirac fermion model for illustration, our results hold for the other systems we tested (Sec. C of Ref. [33]). Effective models often follow from low-energy expansions about a high-symmetry point or band extremum $P$, and can describe important band inversions leading to chiral edge states [6,9,10,12,17,18,22–24]. However, being subspaces of the complete Hilbert space, these models may not have a closed $k$-space manifold (e.g., 2D Brillouin torus). One significant example is the electron valley degree of freedom. The conventional valley Chern number $\bar{\nu}^P$ is usually given by the $k$-space integral of the Berry curvature $F_m$ of filled bands in the vicinity of a valley centered at $P$, integrated to infinity:

$$\bar{\nu}^P = \sum_{i\in\text{filled}} \iint_{k\to\infty} F_i \equiv \sum_{i\in\text{filled}} \bar{C}_i^P. \tag{3}$$

Above, $\bar{C}_i^P$ is the valley Chern number at $P$ per band $|i\rangle$, and the overhead bar indicates that we used the conventional definition of (3) in contrast to the new definition that we will discuss next. Topological quantities like $\bar{\nu}^P$ are only approximately quantized, unless the range of the integral in $k$ is infinite. However, using $\Theta$ instead of $\bar{\nu}^P$ Eq. (3) gives manifestly *quantized* integers using a *finite* loop about $P$. This property may be considered advantageous since we do not need an infinite area of integration. Indeed, the relation to topology becomes clear when we show that the interband index is twice the valley Chern number, i.e., $\Theta = 2\bar{\nu}^P$ in two-band $k \cdot p$ models.

For illustration, consider the 2D gapped Dirac fermion model [36–39], which has a $k \cdot p$ Hamiltonian with integer winding number $w$:

$$\boldsymbol{H}(\boldsymbol{k}) = \begin{pmatrix} \Delta & \alpha|\boldsymbol{k}|^\gamma e^{iw\phi_k} \\ \alpha|\boldsymbol{k}|^\gamma e^{-iw\phi_k} & -\Delta \end{pmatrix}, \tag{4}$$

where the energy gap is $2\Delta$, and $\phi_{\boldsymbol{k}} = \tan^{-1}(k_y/k_x)$.[1] The energy dispersions for the upper ($m$) and lower ($n$) bands are

[1]While $\gamma$ can take on arbitrary integral values in graphene multilayers [37], we note that in monolayer $MoS_2$ and gapped topological

respectively $\pm\sqrt{\Delta^2+\alpha^2|\boldsymbol{k}|^{2\gamma}}$. For a circular loop parameterized as $(k_x, k_y) = (r\cos(\lambda), r\sin(\lambda))$ and centered at the $K'$ point [see Fig. 1(c)], the first three integrals in Eq. (2) conspire to give quantized $\Theta$. The last term in Eq. (2) does not exist in two-band models. As the area of integration approaches the limit $k \to \infty$, the third integral in Eq. (2) contributes less, making $\Theta$ the difference in integrals of $F_m$ and $F_n$. In the $k \to \infty$ limit, these two integrals are just $\bar{C}_m^K$ and $\bar{C}_n^K$. We demonstrate this in Fig. 1(d), where we used $w = 3$, $\Delta = 1$, $\gamma = 1$, and $\alpha = 1$. See Sec. B of Ref. [33] for more on the model's Berry curvature.

To verify $\Theta = 2\bar{\nu}^{K'}$, consider the $k \to \infty$ limit. The Berry curvature sum rule $\sum_i F_i = 0$ gives $F_n = -F_m$ for two-band models. Since $\bar{\nu}^{K'} = \iint F_n$ in this limit, the claim follows from Eq. (2) since the interband frequency integral tends to 0. Indeed, the figure shows $\iint F_n \to -1.5 = \bar{\nu}^{K'}$. With $\Theta = -3$, we verify $\Theta = 2\bar{\nu}^{K'}$.

Next, we discuss $\Theta$ in lattice models. For demonstration, we use Haldane's two-band model for the quantum anomalous Hall effect [36]. However, our results hold for all the models tested in Sec. C of Ref. [33]. On a honeycomb lattice, its Hamiltonian can be written in a Bloch state basis on two sublattices $A, B$, using Pauli matrices $\sigma_i$. Below, $t_1$ is the nearest-neighbor hopping, $t_2$ the amplitude of the complex second-neighbor hopping, $\phi$ the phase accumulated by the $t_2$ hopping, and $M$ the on-site energy between the $A$ and $B$ sublattices. $\boldsymbol{a_i}$ are displacements from a $B$ site to its three nearest-neighbor $A$ sites, and $\boldsymbol{b_i}$ are displacements for nearest-neighbor sites in the same sublattices [40]:

$$\begin{aligned}\boldsymbol{H}(\boldsymbol{k}) = {} & 2t_2\cos\phi\left[\sum_i \cos(\boldsymbol{k}\cdot\boldsymbol{b_i})\right] \\ & + t_1\left[\sum_i [\cos(\boldsymbol{k}\cdot\boldsymbol{a_i})\sigma_1 + \sin(\boldsymbol{k}\cdot\boldsymbol{a_i})\sigma_2]\right] \\ & + \left[M - 2t_2\sin\phi\left(\sum_i \sin(\boldsymbol{k}\cdot\boldsymbol{b_i})\right)\right]\sigma_3. \end{aligned} \tag{5}$$

This model can give topologically nontrivial first Chern numbers that may yield topologically-protected edge states [36]. The Chern number $C = \sum_{i\in\text{filled}} \iint_{k\in\text{FBZ}} F_i$ (where FBZ $\equiv$ first Brillouin zone) changes when the band gap closes and reopens at the high-symmetry points ($K$ or $K'$), as shown in Figs. 2(a) and 2(b). The physics at these valleys is therefore significant, because their gap closings can change the topology, and therefore edge state physics. However, unlike with the Dirac fermion model, it is not easy to define an analogous near-quantized topological quantity at valleys in lattice models. This is because the Berry curvature is not necessarily highly localized at $P$, and the area of the valley available for integration is finite. Therefore quantities like $\bar{\nu}^P$ cannot often be directly acquired from lattice models; at least not without low-energy expansions.

surface states, $\alpha(|\boldsymbol{k}|) \propto |\boldsymbol{k}| = \sqrt{k_x^2 + k_y^2}$ (that is, $\gamma = 1$), and that in biased bilayer graphene, $\alpha(|\boldsymbol{k}|) \propto |\boldsymbol{k}|^2$ ($\gamma = 2$).

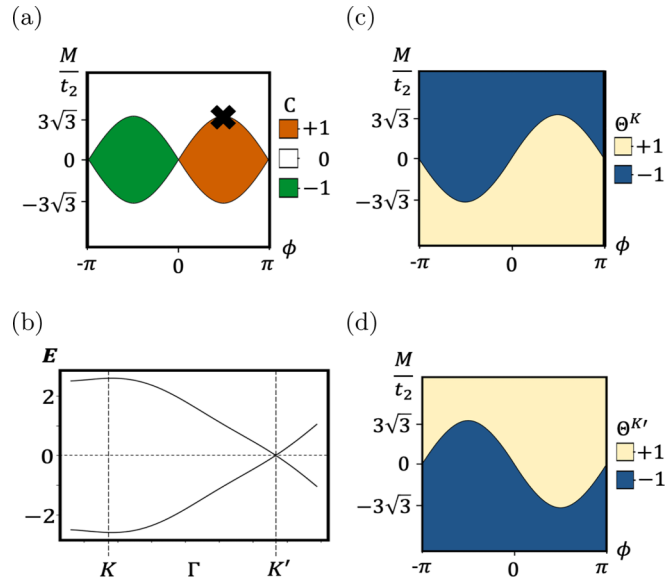


FIG. 2. (a) A phase diagram of the first Chern number $C$ for the Haldane model as a function of $(M, \phi)$. The topological phase transitions occur by gap closures at $K$ or $K'$. (b) Conduction and valence bands of the Haldane model for $M/t_2 = 3\sqrt{3}$, $\phi = \pi/2$, and $t_1 = 4t_2 = 1$. The gap closure at $K'$ corresponds to the phase boundary marked with a cross × in (a). (c) $\Theta^K(M/t_2, \phi)$ using a fixed $k$-space loop of radius 0.2 around the $K$ point (d) $\Theta^{K'}(M/t_2, \phi)$. Notice that $\Theta^K(M/t_2, \phi) + \Theta^{K'}(M/t_2, \phi) = 2C(M/t_2, \phi)$, which is exactly twice the expected phase diagram (a).

However, $\Theta$ can again provide a quantized valley characterization using a small loop centered at $P$. Figures 2(c) and 2(d) show "phase diagrams" analogous to Fig. 2(a) but showing $\Theta$ for each valley. Clearly, when $\Theta^K$ and $\Theta^{K'}$ are summed at each phase space $(M/t_2, \phi)$ point in Figs. 2(c) and 2(d), we recover Haldane's phase diagram Fig. 2(a): $\Theta^K + \Theta^{K'} = 2C$.[2] Hence, compared to the state of the art, we now have a tool to analyze each valley in lattice models without using low-energy expansions.

*Band-resolved topological charge.* The connections between the interband index and local topological characteristics motivate us to define a band-resolved topological charge $\Xi^P$ for each $P$ that would add up to the Chern number $C$. For example, in the Haldane mode, we can define $\Xi^K + \Xi^{K'} \equiv \Theta^K/2 + \Theta^{K'}/2 = C$. This band-resolved topological charge can be generalized to valley and multiband problems. This allows us to not only calculate band-resolved and valley topological indices but also to identify the number and source of edge states from inverting bulk bands without downfolding.

To make this multiband functionality apparent, we use $\Theta_{mn}$ [Eq. (1)] to define the novel generalized band-resolved topological charge $\Xi_i^\gamma$ per band $|i\rangle$, of *context* $\gamma$ (e.g., $\gamma$ could be $P$, such as $K$). For an $N$-level Hamiltonian, the $N$

[2]The factor of 2 is a peculiarity of two-band models that arises from the Berry curvature sum rule $\sum_{i\in\text{all bands}} F_i = 0$, which guarantees us that the Berry curvature at each $k$ point of each band differs only by a sign. Therefore the first two integrals in Eq. (2) simplify to a single integral with a factor of 2 (i.e., either $2\int_{\mathcal{M}} F_n$ or $-2\int_{\mathcal{M}} F_m$).

possible $\Xi_i^\gamma$ values may be found by solving the overdetermined simultaneous equations:

$$\left\{\Theta_{mn}^\gamma = \Xi_n^\gamma - \Xi_m^\gamma, \quad \sum_i \Xi_i^\gamma = 0\right\}. \tag{6}$$

We choose $N-1$ of the $N(N-1)/2$ equations involving $\Theta_{mn}^\gamma$ that make an appropriate linearly independent subset of equations along with $\sum_i \Xi_i^\gamma = 0$, which is a *conservation condition* that resolves linear dependence. This conservation condition is analogous to the Berry curvature sum rule: For a complete basis, the topological charges should sum to 0. Notice that since $\Theta_{mn}^\gamma$ is always an integer, it is reasonable to expect $\Xi_i^\gamma$ to be rational.

Motivated by how $\bar{\nu}^P$ is a sum over filled bands [Eq. (3)], we define:[3]

$$\nu^\gamma = \sum_{i\in\text{filled}} \Xi_i^\gamma. \tag{7}$$

We numerically find that $\Xi_i^\gamma$ and $\nu^\gamma$ are sufficient to calculate the number of edge modes, without using conventional topological quantities such as the Chern number and valley Chern number. By the bulk-edge correspondence, the number of edge modes $b$ due to a domain boundary separating two systems $\alpha$ and $\beta$ is $b = |T^\alpha - T^\beta|$, where $T^\gamma$ is some topological character for context $\gamma$. For example, two adjacent Chern insulators give $b = |C^\alpha - C^\beta|$ [6]. Or, for a domain boundary between two valleys,[4] we have $b = |\nu^K - \nu^{K'}|$ [Eq. (7)] [26,27]. And if the boundary is due to two bulk systems with different external potentials $U_1$ and $U_2$ at the same $P$, we get $b = |\nu^{P,U_1} - \nu^{P,U_2}|$ [26]. Our numerical results shown next support these claims.

We first exemplify the quantities we introduced using the gapped Dirac fermion model [Eq. (4)]. For the example in Fig. 1(d), we use $\Theta = -3$ and solve the simultaneous equations $\{-3 = \Xi_n - \Xi_m, \Xi_n + \Xi_m = 0\}$ [Eq. (6)] to get $\Xi_n = -1.5$ and $\Xi_m = 1.5$, which is consistent with the conventional valley Chern number per band [Eq. (3) $\bar{C}_n^K \approx -1.5$ and $\bar{C}_m^K \approx 1.5$; see Fig. 1(d)].

For a multiband example, consider the eight-band model for gated bilayer graphene including Rashba spin-orbit coupling (Ref. [26]; parameter values in Sec. F of Ref. [33]). As the spin-orbit coupling parameter is tuned from $\lambda_R = 0.2t$ to $0.4t$, we expect a band inversion at the $K$ valley [26], as in Fig. 3(a). For these two values of $\lambda_R$, we present $\Xi_i$ in Table I.

We map the $\Xi_i^{\lambda_R}$ in Table I to existing topological quantities. First, we see that for each choice of $\lambda_R$, $C = \nu^K + \nu^{K'} = 0$, due to $\Xi_i^{\lambda_R,K} = -\Xi_i^{\lambda_R,K'}$. This is consistent with the time-reversal symmetry of the model. We note that the limit of each $\bar{C}_i^P$ may not tend to the quantized $\Xi_i$ in $N$-band models with $N > 2$. To see this, we calculated $\bar{C}_i^P$ at valley $K$ in the $k \to \infty$ limit using Eq. (3). For $\lambda_R = 0.2t$, $(\bar{C}_A^K, \bar{C}_B^K, \bar{C}_C^K, \bar{C}_D^K, \dots) \approx (-0.01, 0.99, -1.99, -0.99, \dots)$. We see that $\bar{C}_A \approx -0.01 \to 0$, which is different from $\Xi_A = -1/2$. This mismatch arises from the last two correction terms in Eq. (2), which do not necessarily tend to 0 in models with $N > 2$ bands.

However, a difference between indices may indicate the number of edge states. Consider a valley problem with a domain boundary between $K$ and $K'$ for fixed $\lambda_R$ at half-filling. From Table I, we have $b = |\nu^K - \nu^{K'}| = |-1-1| = 2$ for $\lambda_R = 0.4t$, and $b = |-2-2| = 4$ for $\lambda_R = 0.2t$. If we instead take a domain boundary problem at $K$ for the two $\lambda_R$ values, we get $b = |\nu^{0.4} - \nu^{0.2}| = |-1-(-2)| = 1$ as the number of edge modes due to the band inversion. These results are consistent with Ref. [26].

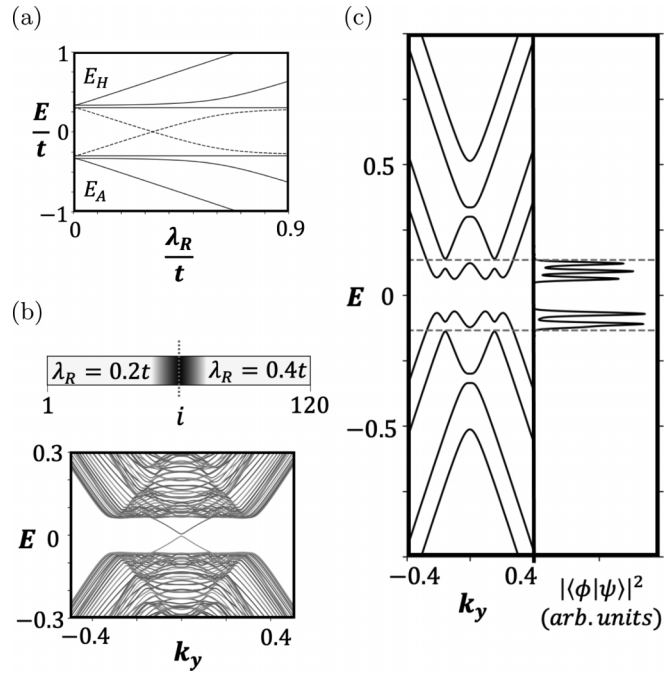


FIG. 3. (a) Band diagram at the $K$ point $(k_x, k_y) = (0, 0)$ for the eight-band bilayer graphene model. At $\lambda_R = 0.2t$, the bands are labeled $E_A, E_B, \dots, E_H$ as we go from $-1$ to $+1$ along the vertical axis. As $\lambda_R$ is varied from $0.2t$ to $0.4t$, the bands $E_D$ and $E_E$ invert at $\lambda_R \approx 0.33t$. (b) (Top) Schematic of real-space nanoribbon with a domain boundary in the $x$ direction separating regions of two different $\lambda_R$. The shaded area represents the calculated wave-function density. (Bottom) Nanoribbon bands at $k_x = 0$ along the $k_y$ direction. (c) (Left) Bulk bands at $k_x = 0$ for $\lambda_R = 0.2t$. (Right) Gaussian-broadened overlap element between bulk and domain boundary band wave functions $|\langle\phi|\psi\rangle|^2$.

TABLE I. $\Xi_i^{\lambda_R}$ for the $K$ valley of the eight-band model for gated bilayer graphene. At $K'$, $\Xi_i^{\lambda_R,K'} = -\Xi_i^{\lambda_R,K}$.

| | $\Xi_A$ | $\Xi_B$ | $\Xi_C$ | $\Xi_D$ | $\Xi_E$ | $\Xi_F$ | $\Xi_G$ | $\Xi_H$ |
|---|---|---|---|---|---|---|---|---|
| $\Xi_i^{0.4}$ | $-\frac{1}{2}$ | $\frac{1}{2}$ | $-\frac{3}{2}$ | $\frac{1}{2}$ | $-\frac{1}{2}$ | $\frac{3}{2}$ | $-\frac{1}{2}$ | $\frac{1}{2}$ |
| $\Xi_i^{0.2}$ | $-\frac{1}{2}$ | $\frac{1}{2}$ | $-\frac{3}{2}$ | $-\frac{1}{2}$ | $\frac{1}{2}$ | $\frac{3}{2}$ | $-\frac{1}{2}$ | $\frac{1}{2}$ |

[3]Recall that we used an overhead bar $\bar{\nu}^P$ in Eq. (3) to denote conventional definitions. $\nu^\gamma$ in Eq. (7) lacks an overhead bar to differentiate our novel contribution, which is quantized as a rational number.

[4]The domain boundary could be between 1D strips separating a $K$ edge from a $K'$ edge. Or within one Brillouin zone, when intervalley scattering is suppressed [5].

We also show that $\Xi_i$ can identify the bulk bands and orbitals causing edge states without explicitly tracking the evolution of spectra [as done in Fig. 3(a)]. Since the only indices that differ between $\lambda_R = 0.4t$ and $\lambda_R = 0.2t$ are $\Xi_D$ and $\Xi_E$, the orbitals causing edge states are from bands $E_D$ and $E_E$. To verify this, we further model a tight-binding nanoribbon of 120 sites that is periodic in the $y$ direction, that has a domain boundary in the $x$ direction at site $i = 60$, as in Fig. 3(b) (top). We discretized the continuum model Eq. (F1) in Sec. F of Ref. [33] to get a tight-binding model that includes both valleys. Our calculations [41] show that edge states accumulate at the domain boundary. We then calculated the nanoribbon bands in Fig. 3(b) (bottom), which shows one zero-energy edge state from each valley. Figure 3(c) shows that these edge states are composed of orbitals from $E_D$ and $E_E$, evident from the large overlap between the zero-energy edge state wave function $|\phi\rangle$ and the bulk wave functions $|\psi\rangle$ of $E_D$ and $E_E$ (calculated in a homogeneous nanoribbon at $\lambda_R = 0.2t$).

*Conclusion and outlook.* We introduced two gauge-invariant quantities, the interband index $\Theta_{mn}$ and band-resolved topological charge $\Xi_i$. These quantized indices offer novel characterizations of topologically significant submanifolds in 2D $k$-space manifolds that are consistent with existing topological characters such as the first and valley Chern numbers. As demonstrated, the differences between $\Xi$ values from different contexts may carry desired physical meaning as the number of edge states. So, the universality and significance of individual $\Xi$ warrant further investigation, as does the interpretation of $\Theta$ and $\Xi$ for loops not enclosing a single $P$ (see Sec. E of Ref. [33]). The non-Abelian version of the interlevel index provided in Ref. [32] may be extended to treat degeneracies, and deserves further work due to the prevalence of accidental and symmetry-protected degeneracies in condensed matter systems. In conclusion, these first-in-literature quantities, due to their elegant quantized nature and broad applicability, are prime candidates for deeper study.

*Acknowledgments.* We acknowledge helpful discussions with Chao Xu from UC San Diego, and with Yafei Ren and Di Xiao from the University of Washington. T.F. acknowledges support from the University of Washington (UW) Physics Department's Provost Fellowship and Graduate Fellowship, the UW Clean Energy Institute's Graduate Fellowship, and the UW Molecular Engineering Materials Center's (MEM-C) Education Fellowship. This work was facilitated through the use of advanced computational, storage, and networking infrastructure provided by the Hyak supercomputer system and funded by UW MEM-C at the University of Washington (DMR-1719797).

[1] M. V. Berry, Quantal phase factors accompanying adiabatic changes, Proc. R. Soc. London A **392**, 45 (1984).
[2] D. J. Thouless, M. Kohmoto, M. P. Nightingale, and M. den Nijs, Quantized Hall Conductance in a Two-Dimensional Periodic Potential, Phys. Rev. Lett. **49**, 405 (1982).
[3] B. Simon, Holonomy, the Quantum Adiabatic Theorem, and Berry's Phase, Phys. Rev. Lett. **51**, 2167 (1983).
[4] M. Nakahara, *Geometry, Topology, and Physics* (CRC press, Boca Raton, FL, 2018).
[5] D. Xiao, M.-C. Chang, and Q. Niu, Berry phase effects on electronic properties, Rev. Mod. Phys. **82**, 1959 (2010).
[6] M. Z. Hasan and C. L. Kane, Colloquium: Topological insulators, Rev. Mod. Phys. **82**, 3045 (2010).
[7] X. Fan, T. Xia, H. Qiu, Q. Zhang, and C. Qiu, Tracking Valley Topology with Synthetic Weyl Paths, Phys. Rev. Lett. **128**, 216403 (2022).
[8] A. Rycerz, J. Tworzydło, and C. Beenakker, Valley filter and valley valve in graphene, Nat. Phys. **3**, 172 (2007).
[9] J. Jung, F. Zhang, Z. Qiao, and A. H. MacDonald, Valley-Hall kink and edge states in multilayer graphene, Phys. Rev. B **84**, 075418 (2011).
[10] F. Zhang, J. Jung, G. A. Fiete, Q. Niu, and A. H. MacDonald, Spontaneous Quantum Hall States in Chirally Stacked Few-Layer Graphene Systems, Phys. Rev. Lett. **106**, 156801 (2011).
[11] D. Xiao, W. Yao, and Q. Niu, Valley-Contrasting Physics in Graphene: Magnetic Moment and Topological Transport, Phys. Rev. Lett. **99**, 236809 (2007).
[12] A. H. Castro Neto, F. Guinea, N. M. R. Peres, K. S. Novoselov, and A. K. Geim, The electronic properties of graphene, Rev. Mod. Phys. **81**, 109 (2009).
[13] R. Gorbachev, J. Song, G. Yu, A. Kretinin, F. Withers, Y. Cao, A. Mishchenko, I. Grigorieva, K. S. Novoselov, L. Levitov *et al.*, Detecting topological currents in graphene superlattices, Science **346**, 448 (2014).
[14] X. Xu, W. Yao, D. Xiao, and T. F. Heinz, Spin and pseudospins in layered transition metal dichalcogenides, Nat. Phys. **10**, 343 (2014).
[15] K. F. Mak, K. L. McGill, J. Park, and P. L. McEuen, The valley Hall effect in $MoS_2$ transistors, Science **344**, 1489 (2014).
[16] G. W. Semenoff, V. Semenoff, and F. Zhou, Domain Walls in Gapped Graphene, Phys. Rev. Lett. **101**, 087204 (2008).
[17] I. Martin, Y. M. Blanter, and A. F. Morpurgo, Topological Confinement in Bilayer Graphene, Phys. Rev. Lett. **100**, 036804 (2008).
[18] W. Yao, S. A. Yang, and Q. Niu, Edge States in Graphene: From Gapped Flat-Band to Gapless Chiral Modes, Phys. Rev. Lett. **102**, 096801 (2009).
[19] J. Li, A. F. Morpurgo, M. Büttiker, and I. Martin, Marginality of bulk-edge correspondence for single-valley Hamiltonians, Phys. Rev. B **82**, 245404 (2010).
[20] J. Li, I. Martin, M. Büttiker, and A. F. Morpurgo, Topological origin of subgap conductance in insulating bilayer graphene, Nat. Phys. **7**, 38 (2011).
[21] Z. Qiao, J. Jung, Q. Niu, and A. H. MacDonald, Electronic highways in bilayer graphene, Nano Lett. **11**, 3453 (2011).
[22] F. Zhang, A. H. MacDonald, and E. J. Mele, Valley chern numbers and boundary modes in gapped bilayer graphene, Proc. Natl. Acad. Sci. USA **110**, 10546 (2013).
[23] A. Vaezi, Y. Liang, D. H. Ngai, L. Yang, and E.-A. Kim, Topological Edge States at a Tilt Boundary in Gated Multilayer Graphene, Phys. Rev. X **3**, 021018 (2013).

[24] L. Ju, Z. Shi, N. Nair, Y. Lv, C. Jin, J. Velasco, C. Ojeda-Aristizabal, H. A. Bechtel, M. C. Martin, A. Zettl *et al.*, Topological valley transport at bilayer graphene domain walls, Nature **520**, 650 (2015).

[25] J. Li, K. Wang, K. J. McFaul, Z. Zern, Y. Ren, K. Watanabe, T. Taniguchi, Z. Qiao, and J. Zhu, Gate-controlled topological conducting channels in bilayer graphene, Nat. Nanotechnol. **11**, 1060 (2016).

[26] Z. Qiao, X. Li, W.-K. Tse, H. Jiang, Y. Yao, and Q. Niu, Topological phases in gated bilayer graphene: Effects of Rashba spin-orbit coupling and exchange field, Phys. Rev. B **87**, 125405 (2013).

[27] M. Ezawa, Symmetry protected topological charge in symmetry broken phase: Spin-Chern, spin-valley-Chern and mirror-Chern numbers, Phys. Lett. A **378**, 1180 (2014).

[28] E. Fradkin, *Field Theories of Condensed Matter Physics* (Cambridge University Press, Cambridge, 2013).

[29] P.-O. Löwdin, A note on the quantum-mechanical perturbation theory, J. Chem. Phys. **19**, 1396 (1951).

[30] J. M. Luttinger and W. Kohn, Motion of electrons and holes in perturbed periodic fields, Phys. Rev. **97**, 869 (1955).

[31] G. L. Bir, G. E. Pikus *et al.*, *Symmetry and Strain-Induced Effects in Semiconductors* (Wiley New York, 1974), Vol. 484.

[32] C. Xu, J. Wu, and C. Wu, Quantized interlevel character in quantum systems, Phys. Rev. A **97**, 032124 (2018).

[33] See Supplemental Material at http://link.aps.org/supplemental/10.1103/PhysRevB.108.L081111 for a derivation of the interband frequency; more details on the Berry curvature of the gapped Dirac fermion model (4); a list of models we tested; more definitions of topological indices (first, valley, spin, and spin-valley Chern numbers); a proof for showing $\Theta^{mn} = -\Theta^{nm}$; a discussion on the choice of $k$-space loops; and details of the eight-band bilayer graphene model, along with computational details.

[34] T. Holder, D. Kaplan, and B. Yan, Consequences of time-reversal-symmetry breaking in the light-matter interaction: Berry curvature, quantum metric, and diabatic motion, Phys. Rev. Res. **2**, 033100 (2020).

[35] S. Kitamura, N. Nagaosa, and T. Morimoto, Nonreciprocal Landau–Zener tunneling, Commun. Phys. **3**, 63 (2020).

[36] F. D. M. Haldane, Model for a Quantum Hall Effect without Landau Levels: Condensed-Matter Realization of the "Parity Anomaly", Phys. Rev. Lett. **61**, 2015 (1988).

[37] X. Zhang, W.-Y. Shan, and D. Xiao, Optical Selection Rule of Excitons in Gapped Chiral Fermion Systems, Phys. Rev. Lett. **120**, 077401 (2018).

[38] X. Zhang, Topological effects in two-dimensional systems, Ph.D. thesis, Carnegie Mellon University, 2019.

[39] M. S. Dresselhaus, G. Dresselhaus, and A. Jorio, *Group Theory: Application to the Physics of Condensed Matter* (Springer Science & Business Media, 2007).

[40] M. Fruchart and D. Carpentier, An introduction to topological insulators, C. R. Phys. **14**, 779 (2013).

[41] C. W. Groth, M. Wimmer, A. R. Akhmerov, and X. Waintal, Kwant: A software package for quantum transport, New J. Phys. **16**, 063065 (2014).